An infrared flash contemporaneous with the γ-rays of GRB 041219a

C. H. Blake[1], J. S. Bloom[1,2], D. L. Starr[13], E. E. Falco[3], M. Skrutskie[9], E. E. Fenimore[7], G. Duchêne[12], A. Szentgyorgyi[3], S. Hornstein[10], J. X. Prochaska[4], C. McCabe[11], A. Ghez[10], Q. Konopacky[10], K. Stapelfeldt[11], K. Hurley[5], R. Campbell[6], M. Kassis[6], F. Chaffee[6], N. Gehrels[8], S. Barthelmy[8], J. R. Cummings[8], D. Hullinger[8,14], H. A. Krimm[8,15], C. B. Markwardt[8,14], D. Palmer[7], A. Parsons[8], K. McLean[7] & J. Tueller[8]

[1]*Harvard College Observatory, Cambridge, Massachusetts 02138, USA*
[2]*Astronomy Department, University of California at Berkeley, Berkeley, California 94720, USA*
[3]*Smithsonian Astrophysical Observatory, Cambridge, Massachusetts 02138, USA*
[4]*UCO/Lick Observatory, Santa Cruz, California 95064, USA*
[5]*Space Sciences Laboratory, University of California, Berkeley, California 94720, USA*
[6]*W.M. Keck Observatories, Kamuela, Hawaii 96743, USA*
[7]*Los Alamos National Laboratory, Los Alamos, New Mexico 87545, USA*
[8]*NASA Goddard Space Flight Center, Greenbelt, Maryland 20771, USA*
[9]*University of Virginia, Department of Astronomy, Charlottesville, Virginia 22904, USA*
[10]*University of California, Los Angeles, Los Angeles, California 90095, USA*
[11]*Jet Propulsion Laboratory, California Institute of Technology, Pasadena, California 91109, USA*
[12]*Laboratoire d'Astrophysique, Observatoire de Grenoble, 38041 Grenoble Cedex 9, France*
[13]*Gemini Observatory, Hilo, Hawaii 96720, USA*
[14]*University of Maryland, College Park, Maryland 20742, USA*
[15]*Universities Space Research Association, Columbia, Maryland 21044, USA*

The explosion that results in a cosmic γ-ray burst (GRB) is thought to produce emission from two physical processes: the central engine gives rise to the high-energy emission of the burst through internal shocking[1], and the subsequent interaction of the flow with the external environment produces long-wavelength afterglows[2–4]. Although observations of afterglows[5] continue to refine our understanding of GRB progenitors and relativistic shocks, γ-ray observations alone have not yielded a clear picture of the origin of the prompt emission[6] nor details of the central engine. Only one concurrent visible-light transient has been found[7] and it was associated with emission from an external shock. Here we report the discovery of infrared emission contemporaneous with a GRB, beginning 7.2 minutes after the onset of GRB 041219a (ref. 8). We acquired 21 images during the active phase of the burst, yielding early multi-colour observations. Our analysis of the initial infrared pulse suggests an origin consistent with internal shocks.

Prompt long-wavelength afterglow emission is predicted to arise when the reverse (external) shock encounters the ejecta of the explosion[2,3], or through γ-ray heating of the circumburst material[4]. Indeed, four GRBs[7,9–12] have exhibited transient optical emission that could be associated with reverse shocks, but early-time optical transients have not been found for the vast majority of bursts (however, new larger-aperture robotic optical systems have met with increasing success). As even moderate levels of dust near the GRB or along the line-of-sight in the host galaxy could effectively suppress detectable optical emission[13], contemporaneous observations at infrared (IR) wavelengths, where light suppression is relatively minimized, offer a natural means to uncover any prompt emission. This was one motivation for our construction of the Peters Automated Infrared Imaging Telescope (PAIRITEL; Fig. 1). At 1.3 m in diameter, it is one of the largest, completely autonomous telescope systems in the world and one of only a few capable of imaging at IR wavelengths (1.1–2.3 μm; see ref. 14). PAIRITEL acquires images with high temporal cadence (integration times of 7.8 s) in three colours simultaneously. The field of view is rather large, $8.5' \times 8.5'$, for IR imaging, allowing for follow-up of GRB localizations of even modest precision.

GRB 041219a triggered the IBIS instrument on board the INTEGRAL[15] satellite on 19 December 2004 at 01:42:54 UTC, which was reported at 01:44:05 UTC. The initial position of right ascension (RA) 00 h 24 min 26 s, declination (dec.) $+62°\ 50'\ 06''$ was refined to $2'$ uncertainty at 01:47:49 UTC and a final offline location[8] was reported at 03:31:58 UTC. The Burst Alert Telescope (BAT) on the Swift satellite[16] triggered and located GRB 041219a on board at 01:42:18 UTC with a position that was within $4'$ of the IR source. If Swift had not still been in its commissioning phase with slewing disabled, the spacecraft could have slewed to the location within 70 s of the BAT trigger. The ground-based BAT location (RA 00 h 24 min 37.0 s, dec. $+62°\ 50'\ 49.2''$) was within $48''$ of the IR source. As viewed by BAT, the burst duration (Δt) above background was 520 s and was very bright, with up to 6.5×10^4 counts s^{-1} (unsaturated) between 15 and 350 keV and a fluence of 1.15×10^{-4} erg cm^{-2}. The time evolution of the count rate in four BAT channels covering 15 to 350 keV is reproduced in Fig. 2.

PAIRITEL began to slew on 19 December 2004, 01:48:20 UTC, and the first observations of the GRB field commenced 58 s later. Despite very poor observing conditions (sustained 40 m.p.h. winds, variable sky transmission, and $4''$ seeing), comparison of the first epoch of data revealed a new, variable source[17] not visible in the 2MASS (Two Micron All Sky Survey) catalogue images of the field. When compared to the astrometric grid of 2MASS stars in the field, we find the absolute position of the IR transient (IRT) to be RA 00 h 24 min 27.68 s ± $0.124''$, dec. $+62°\ 50'\ 33.501''$ ± $0.228''$, with its uncertainty dominated by the mapping to 2MASS catalogue stars. An optical flash was also detected by the RAPTOR experiment during the prompt γ-ray emission[18].

PAIRITEL observations of the transient continued over the following three nights, until inclement weather in Arizona precluded additional observations. In total, 5,790 images were acquired by the system over these nights. In addition, we obtained deep J-band imaging on 20 and 21 December UTC using the NIRC-1[19] instrument on the Keck I 10-m telescope on Mauna Kea, Hawaii. Consistent within the astrometric accuracy of the IRT from 19 December, we found a point-like source in J-band (Fig. 1). Over these two nights, that source was seen to fade by 1.0 mag, confirming its identification with the IRT. The Keck images revealed two sources within $2.5''$ of the transient position (S1; $J \approx 19.7$ mag, $2.5''$ north-north-east: S2: $J \approx 21.4$ mag, $1.5''$ east): both were unresolved apparent point sources. The source S1 is bright enough to contaminate the PAIRITEL J-band aperture photometry on 21 December, which accounts for the difference between our measurements and the fainter measurements[20] from Apache Point Observatory (APO) and Keck on the same date. When comparing PAIRITEL photometry with higher-resolution Keck and APO results for 21 December, the flux from S1+S2 appears to be a 51% contamination in H band, 58% in J band, and has negligible contribution in the K_s band.

The resulting light curves (see Supplementary Table 1) shown in Fig. 3 reveal a complex time history of the afterglow. The first six PAIRITEL exposures at $t + 7.2$ min after the trigger show a source that brightens, then fades very rapidly in all filters by about $t + 9$ min, and then rebrightens by $t + 20$ min. Using our data and data reported in the literature, we fitted the light curves as the sum of three smoothly connected rise and fall brightening events; the results of these fits are shown in Fig. 3. During the first few days, the source colours, though rather uncertain, appear consistent with a single value of the spectral slope of $\beta \approx 0.4$ (Fig. 4). Additionally, there is some evidence that the IRT was redder during the 'flash' event at $t + 7.2$ min.

How might the light curve be understood as emission from the reverse and forward shock? The electrons in the shock are assumed to be accelerated to a power-law spectrum with number density as a function of energy (E) proportional to E^{-p}. In a constant-density circumburst environment, a reverse shock is expected[21] to rise rapidly ($\alpha = 3p - 3/2$, with flux density $f_\nu \propto t^\alpha$) and then, in the 'thin shell' case (see below), decline with $\alpha = -(27p + 7)/35 \approx -2$ after the emission peak, corresponding to the time ($t_\times$) that the reverse shock crosses the explosion ejecta. The IR emission from the forward shock[22] should rise slowly as $\alpha = 0.5$, then decline as $\alpha = 3(1 - p)/4$. Associating peak 2 with the reverse shock and peak 3 with the forward shock, we find reasonable agreement, to within the measurement uncertainties, of the data with this model. In particular, the three implied values for p (2.5 ± 1.1, 4.2 ± 4.1, 2.6 ± 0.2, for the reverse-rise, reverse-decline, and forward-decline, respectively) are all consistent with the usual range[5] of $p = 2.2$–2.5. A consequence of this interpretation is that, in the absence of effects due to collimation of the burst, radio afterglow emission should be dominated by a rising reverse shock, peaking at time $t = (10.2 \pm 1.8)(\nu/8.4)^{-35/54}$ d where ν is in GHz; this is thus far confirmed with reports of rising radio emission at least to day 2.9 (ref. 23).

With this interpretation, there are three puzzles. First, we would expect[3] the source to have become bluer during the forward shock rise, which is not required (though is not excluded) by our data. The second puzzle concerns the timing of the reverse shock peak relative to the GRB duration. We expect[24,25] $t_\times = 1{,}670\ \mathrm{s} > \Delta t$ only when Δt is less than the time when the shock begins to decelerate (commonly deemed the 'thin shell' case). This deceleration time occurs when the shock has swept up from the circumburst environment a quantity $1/\Gamma_0$ times the entrained mass, where Γ_0 is the terminal Lorentz factor of the shock. A delayed reverse shock crossing time requires $\Gamma_0 < 67 E_{52}^{1/8} n^{-1/8} (\Delta t/520)^{-3/8} [0.5(1+z)]^{3/8}$, where n is the circumburst particle density in units of baryons cm^{-3}, E_{52} is the energy in the shock in units of 10^{52} erg, Δt is in units of seconds and the redshift of the burst is z. This initial Lorentz factor constraint is uncomfortably smaller than the limits placed on previous values[25] of Γ_0, which suggests that either the burst occurred at high redshift (which is excluded by the RAPTOR detection[18]), was exceptionally energetic, or occurred in a low-density environment. Alternatively, the observed variability could be due to inhomogeneous density structure in the circumburst environment or delayed energy injection into the blastwave.

The third and most intriguing puzzle is the physical origin of the IR flash at $t_1 = 462$ s that has marginal evidence for appearing more red than the afterglow at later times (here the subscript 1 refers to the first peak in the light curve). Regardless of the interpretation of events 2 and 3, the rapid rise and fall appear to preclude an association with a reverse shock: the fit of a power-law decay slope to the K_s data acquired less than 10 min from burst trigger yields $\alpha = -18 \pm 5$, whereas setting $\alpha = -2$, as expected of a reverse shock, yields an unacceptable fit (reduced $\chi^2 = 4.4$). The duration of the IR flash ($\delta t \approx 45$ s, taken as the full-width at half-maximum of the model fit to the data) is comparable to the widths of the largest timescale for substructure in γ-rays; indeed, this δt is remarkably similar to that of the optical pulse[7] in GRB 990123. The

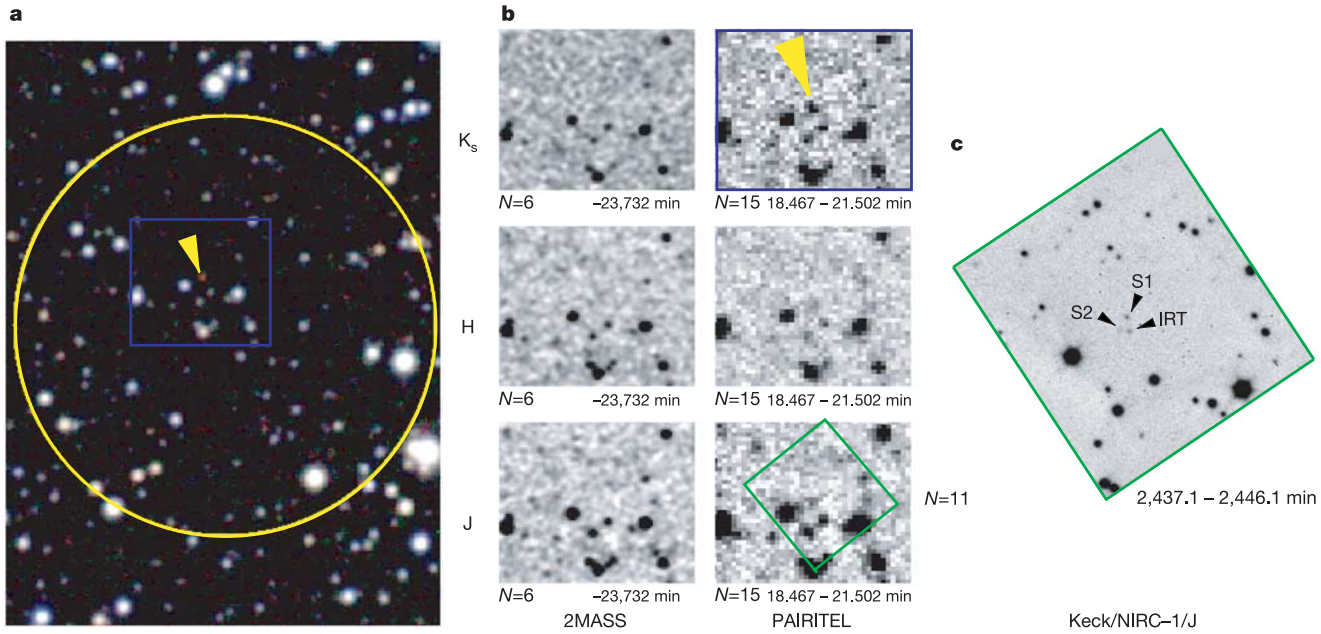

Figure 1 Images of the IR flash associated with GRB 041219a. The discovery was made with PAIRITEL, located atop Mt Hopkins, Arizona. Normally, the telescope's observing plan is autonomously scheduled before nightfall by a routine that optimizes the preset priorities and scheduling constraints of all objects in the PAIRITEL database. When the new GRB alert was received, a series of observations were automatically inserted into the observing queue and the telescope began to slew to the target field. Left **a**, false-colour image of the IR flash (yellow arrow) of GRB 041219a inside the 2′ (90% confidence) INTEGRAL error region[8] (yellow circle). At early times, the source is the reddest object in the field, indicative of very high extinction due to dust in the disk of our Galaxy. **b**, the Two Micron All Sky Survey (2MASS) images of the field from 2000 June 15 UTC compared with the three colour images showing the infrared transient (IRT) several minutes after the GRB triggered. Time relative to the GRB trigger is given, as is the number (N) of individual images combined. The individual 2MASS images are 1.3-s integrations, so the combination of six 2MASS images is equal to a single PAIRITEL image. The 2MASS and PAIRITEL fields are centred on the IRT and are approximately 1′ on a side (shown as a blue box in **a**). A local background from a two-dimensional median was subtracted from all images to remove large-scale background variations. For all images, north is up and east is to the left. **c**, the Keck NIRC-1[19] imaging at J-band on December 21 UTC, in the same region as the PAIRITEL images. NIRC-1 images were combined in the usual manner and the combined images had a seeing of less than 0.8″ on both nights. The IRT, as well as two unresolved nearby sources (S1, S2), are labelled.

ratio of the width to the time after trigger $t \approx 462$ s, $\delta t/t = 0.10$, is similar to that seen in individual pulses in bright GRBs[26] but a factor of ~10 smaller than the $\delta t/t$ of the optical flash of GRB 990123.

We suggest, therefore, that the origin of the first peak is from the internal shock that itself produced the GRB. Such emission is possible if the synchrotron cooling frequency from the internal shock emission is well below γ-ray frequencies[3]. Indeed, if the IR emission is due to internal shocks, then the observed flash may be due to a superposition of several unresolved shorter-timescale pulses. Future observations of IR flashes in the Swift era will no doubt test the ubiquity and nature of rapidly variable early-time emission as reported here.

Note added in proof: Some of our additional independent photometric analyses of the first event also reveal a rapid decline but show less evidence for a rapid rise than shown in Fig. 2. Since we based our conclusions on the nature of that event primarily on the later-time

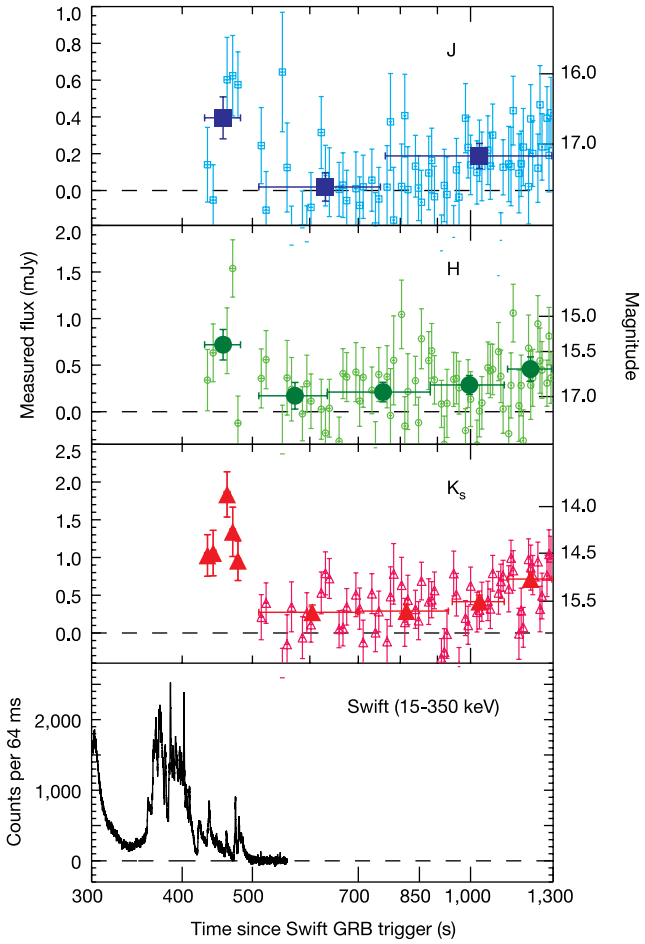

Figure 2 Evolution of the IR flash associated with GRB 041219a. We argue that the initial pulse is not traditional afterglow from an external shock but instead related to the internal shocks of the central engine. Shown (top three panels) are measurements derived from individual 7.8-s exposures as small, light-coloured points, and detections from stacks of images as heavy, dark-coloured points; error bars are 1σ, estimated from photon noise and the distribution of randomly placed apertures on the images. Also plotted (bottom panel) is the light curve from the 15–350-keV channels of the BAT instrument aboard Swift. Data reduction was as follows: the response to variable sky and bias in the detectors was estimated for each exposure in each band by median-combining all the exposures taken within a two to four minute window. A flat-field correction for fixed pixel-to-pixel variations in detector gain was made using images of the dawn sky. Subtracting the dark + sky response and normalizing by the flat-field produced a reduced image. Reduced images were measured either individually or as stacks of co-added images. As individual images undersample the seeing owing to atmospheric blurring, photometry was performed differentially in an aperture of fixed size. All of the images were aligned to a common reference image to an accuracy of approximately 0.1 pixel. Images were measured individually or in stacks created by summing individual images with weights determined by the signal-to-noise of each image. The measured flux at the position of the GRB was compared to the flux measured for a set of nearby comparison stars. Magnitudes of the comparison stars are known to a high accuracy (2%) from the 2MASS catalogue. PAIRITEL uses the same detectors and filters as 2MASS, so our differential photometry is expected to be free from systematic offsets.

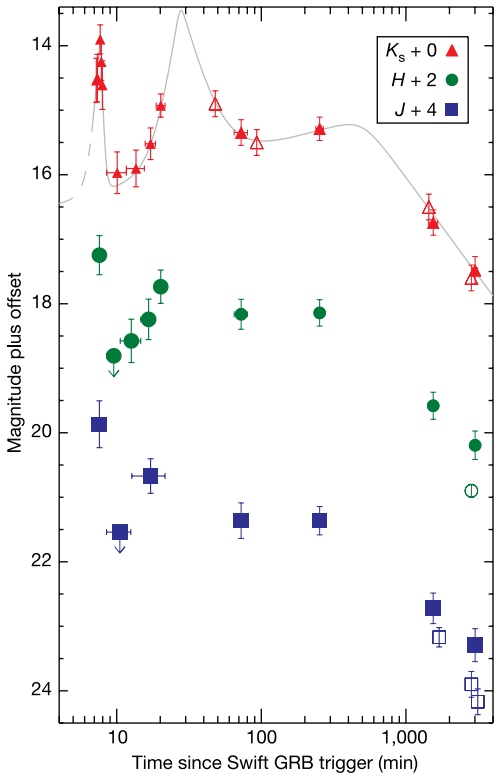

Figure 3 Long-timescale variability of the IR transient associated with GRB 041219a. The K_s-band light curve is reasonably fitted (grey curve) as a sum of three power-law rise and fall events with peaks at times since the burst $[t_1, t_2, t_3] = [7.73 \pm 0.14$ min, 27.5 ± 4.9 min, ≈500 min] and specific brightness $[f_\nu(t_1), f_\nu(t_2), f_\nu(t_3)] = [1.6 \pm 0.3$ mJy, 2.5 ± 2.8 mJy, 0.5 ± 0.1 mJy]. The rise and fall near the second peak is fitted by $\alpha_{2,r} = 6.1 \pm 2.9$ ($\alpha_{2,f} = -3.4 \pm 2.8$), with the specific brightness changing as $f_\nu \propto t^\alpha$. The final rise and fall parameters depend on the poorly constrained value of t_3. Fixing $t_3 = 500$ min, we find $\alpha_{3,r} = 0.3 \pm 0.1$ and $\alpha_{3,f} = -1.2 \pm 0.1$. The first peak has both rapid rise and fall times (see text). The global χ^2 per degree of freedom (d.f.) is an acceptable 1.24. The reported 1σ parameter uncertainties do not reflect the covariance between the parameter fits. Additionally, all of these derived values depend on the choice of a smoothing parameter to connect the two power-laws (s in equation (2) of ref. 27; here, we chose $s = 5$). The J- and H-band light curves are consistent with the K_s-band shape, apart from the overall flux normalization. Photometry was performed as follows: large numbers of individual exposures were combined with sub-pixel sampling and produced a high signal-to-noise, high-resolution image for each epoch. The point-spread function in these images is well sampled, so the technique of difference image photometry was utilized. The uncertainty in the differential fluxes of the IRT between individual epochs is near photon-limited. The differential fluxes are converted to magnitudes from aperture photometry at the position of the IRT in the late-time (21 December) reference image. Other data, plotted as open points, include two J-band observations made with the Keck I telescope, JHK_s observations from Apache Point Observatory[20], and three K_s measurements (see ref. 28 and references therein) from Mt Palomar.

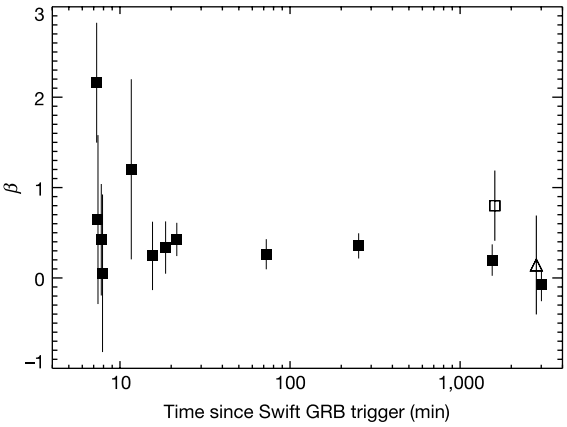

Figure 4 Colour evolution of the afterglow of GRB 041219a, corrected for extinction due to interstellar dust. The dust extinction[29] at the location of GRB 041219a is high: A(V band) = 5.9 (and highly uncertain). Using a common dust extinction law ($R_V = 3.1$), the extinction in magnitudes is A(J) = 1.6, A(H) = 1.04, and $A(K_s) = 0.66$. We fitted (filled squares) for a spectral index β with our J, H and K_s measurements at each epoch using the flux relation $F_\nu(t) = F_0(t)(\lambda_c/\lambda_H)^\beta$, where λ_c is the central wavelength of the filter bandpasses (c = [J, H, K]). Including the z-band detection[30] ($\lambda_c \approx 9{,}100$ Å) that was nearly coeval with our IR observations results in a steeper spectral slope of 0.80 ± 0.39 (open square) than found with the IR data alone. Our fit to the Apache Point JHK data[20] is also shown with an open triangle. With fits that yielded χ^2/d.f. greater than unity, we scale the resulting 1σ errors by $\sqrt{\chi^2}$/d.f. Though there is some evidence for secular trends, the resulting values for β are consistent with a single value of $\beta \approx 0.4$. We caution, however, that this common value of the spectral index is strongly dependent upon the assumed dust column. For different values of the extinction, A(V) = 4.0 and A(V) = 7.0, the fits to the spectral index are $\beta \approx 0.7$ and $\beta \approx 0.2$, respectively. Indeed, the standard forward-shock model[22] tends to favour a larger value ($\beta \approx 0.55$) than found with the IR data alone. For the first peak (during the GRB), there is marginal evidence that the source is intrinsically redder than at later times.

imaging and the rapid fall behaviour, the interpretation is largely unchanged by various analyses. □

Received 12 January; accepted 1 March 2005; doi:10.1038/nature03520.

1. Fenimore, E. E., Madras, C. D. & Nayakshin, S. Expanding relativistic shells and gamma-ray burst temporal structure. *Astrophys. J.* **473,** 998 (1996).
2. Mészáros, P. & Rees, M. J. Optical and long-wavelength afterglow from gamma-ray bursts. *Astrophys. J.* **476,** 232–237 (1997).
3. Sari, R. & Piran, T. Predictions for the very early afterglow and the optical flash. *Astrophys. J.* **520,** 641–649 (1999).
4. Beloborodov, A. M. Radiation front sweeping the ambient medium of gamma-ray bursts. *Astrophys. J.* **565,** 808–828 (2002).
5. van Paradijs, J., Kouveliotou, C. & Wijers, R. A. M. J. Gamma-ray burst afterglows. *Annu. Rev. Astron. Astrophys.* **38,** 379–425 (2000).
6. Baring, M. G. & Braby, M. L. A study of prompt emission mechanisms in gamma-ray bursts. *Astrophys. J.* **613,** 460–476 (2004).
7. Akerlof, C. *et al.* Observation of contemporaneous optical radiation from a gamma-ray burst. *Nature* **398,** 400–402 (1999).
8. Gotz, D., Mereghetti, S., Shaw, S., Beck, M. & Borkowski, J. GRB 041219—A long GRB detected by INTEGRAL. *GCN Circ.* 2866 (2004).
9. Fox, D. W. *et al.* Early optical emission from the γ-ray burst of 4 October 2002. *Nature* **422,** 284–286 (2003).
10. Fox, D. W. *et al.* Discovery of early optical emission from GRB 021211. *Astrophys. J.* **586,** L5–L8 (2003).
11. Li, W., Filippenko, A. V., Chornock, R. & Jha, S. The early light curve of the optical afterglow of GRB 021211. *Astrophys. J.* **586,** L9–L12 (2003).
12. Rykoff, E. S. *et al.* The early optical afterglow of GRB 030418 and progenitor mass loss. *Astrophys. J.* **601,** 1013–1018 (2004).
13. Klose, S. *et al.* The very faint K-band afterglow of GRB 020819 and the dust extinction hypothesis of the dark bursts. *Astrophys. J.* **592,** 1025–1034 (2003).
14. Zerbi, F. M. *et al. Proc. SPIE* **4841,** 737–748 (2003).
15. Winkler, C. *et al.* The INTEGRAL mission. *Astron. Astrophys.* **411,** L1–L6 (2003).
16. Gehrels, N. *et al.* The Swift gamma-ray burst mission. *Astrophys. J.* **611,** 1005–1020 (2004).
17. Blake, C. & Bloom, J. S. GRB 041219: Infrared afterglow candidate. *GCN Circ.*, 2870 (2004).
18. Vestrand, W. T. *et al.* A link between prompt optical and prompt γ-ray emission in γ-ray bursts. *Nature* doi:10.1038/nature03515 (this issue).
19. Matthews, K., Soifer, B. T. & McLean, I. in *Infrared Astronomy with Arrays, the Next Generation* (ed. McLean, I.) 239 (Kluwer, Dordrecht, 1994).
20. Hearty, F. *et al.* NIR observations of GRB 041219. *GCN Circ.* 2916 (2004).
21. Kobayashi, S. Light curves of gamma-ray burst optical flashes. *Astrophys. J.* **545,** 807–812 (2000).
22. Sari, R., Piran, T. & Narayan, R. Spectra and light curves of gamma-ray burst afterglows. *Astrophys. J.* **497,** L17–L20 (1998).
23. van der Horst, A., Rol, E. & Strom, R. GRB 041219: Second epoch WSRT radio observations. *GCN Circ.*, 2895 (2004).
24. Sari, R. Hydrodynamics of gamma-ray burst afterglow. *Astrophys. J.* **489,** L37–L40 (1997).
25. Zhang, B., Kobayashi, S. & Mészáros, P. Gamma-ray burst early optical afterglows: Implications for the initial Lorentz factor and the central engine. *Astrophys. J.* **595,** 950–954 (2003).
26. Ramirez-Ruiz, E. & Fenimore, E. E. Pulse width evolution in gamma-ray bursts: Evidence for internal shocks. *Astrophys. J.* **539,** 712–717 (2000).
27. Nakar, E. & Piran, T. Early afterglow emission from a reverse shock as a diagnostic tool for gamma-ray burst outflows. *Mon. Not. R. Astron. Soc.* **353,** 647–653 (2004).
28. Moon, D.-S., Cenko, B. & Adams, J. GRB041219: Continued NIR observations. *GCN Circ.* 2884 (2004).
29. Schlegel, D. J., Finkbeiner, D. P. & Davis, M. Maps of dust infrared emission for use in estimation of reddening and cosmic microwave background radiation foregrounds. *Astrophys. J.* **500,** 525–553 (1998).
30. Cenko, S. B. GRB 041219: Optical afterglow detection. *GCN Circ.* 2885 (2004).

Supplementary Information accompanies the paper on **www.nature.com/nature**.

Acknowledgements J.S.B. was supported by a Junior Fellowship from the Harvard Society of Fellows. PAIRITEL was made possible by a grant from the Harvard Milton Fund. Additional funding from the Smithsonian Institution for the PAIRITEL project is acknowledged. We thank the entire Mt Hopkins Ridge staff for support of PAIRITEL, especially W. Peters, R. Hutchins and T. Groner. J. Huchra is thanked for stewardship of the telescope under adverse conditions in the week leading up to GRB 041219a. This publication makes use of data products from the Two Micron All Sky Survey (2MASS), which is a joint project of the University of Massachusetts and the Infrared Processing and Analysis Center/California Institute of Technology, funded by the National Aeronautics and Space Administration and the National Science Foundation.

Competing interests statement The authors declare that they have no competing financial interests.

Correspondence and requests for materials should be addressed to J.S.B. (jbloom@astro.berkeley.edu).

Albedo of the south pole on Mars determined by topographic forcing of atmosphere dynamics

Anthony Colaprete[1], Jeffrey R. Barnes[2], Robert M. Haberle[1], Jeffery L. Hollingsworth[3], Hugh H. Kieffer[4] & Timothy N. Titus[4]

[1]*NASA Ames Research Center, Space Science Division, Moffett Field, Mountain View, California 94035, USA*
[2]*College of Oceanic and Atmospheric Sciences, Oregon State University, Corvallis, Oregon 97331, USA*
[3]*San José State University Foundation, NASA Ames Research Center, Moffett Field, Mountain View, California 94035, USA*
[4]*US Geological Survey, Astrogeology Team, Flagstaff, Arizona 86001, USA*

The nature of the martian south polar cap has remained enigmatic since the first spacecraft observations[1–6]. In particular, the presence of a perennial carbon dioxide ice cap, the formation of a vast area of black 'slab ice' known as the Cryptic region and the asymmetric springtime retreat of the cap have eluded explanation. Here we present observations and climate modelling that indicate the south pole of Mars is characterized by two distinct regional climates that are the result of dynamical forcing by the largest southern impact basins, Argyre and Hellas. The style of surface frost deposition is controlled by these regional climates. In the cold and stormy conditions that exist poleward of 60° S and extend 180° in longitude west from the Mountains of Mitchel (~30° W), surface frost accumulation is dominated by precipitation. In the opposite hemisphere, the polar atmosphere is relatively warm and clear and frost accumulation is dominated by direct vapour deposition. It is the differences in these deposition styles that determine the cap albedo.